ACS APPLIED MATERIALS & INTERFACES

www.acsami.org

Research Article

Self-Assembly of Hemimyzon Formosanus-Inspired Crescent-Shaped Nanosucker Arrays for Reversible Adhesion

Jung-Hsuan Hsu,[†] Nien-Ting Tang,[†] Ting-Fang Hsu, Shin-Hua Lin, Cai-Yin Fang, Yun-Wen Huang, and Hongta Yang*

Cite This: *ACS Appl. Mater. Interfaces* 2023, 15, 56203−56212

Read Online

ACCESS | Metrics & More | Article Recommendations | Supporting Information

ABSTRACT: Hemimyzon formosanus, a species of ray-finned fish, makes use of crescent-shaped abdominal suckers for adhering to irregular, rough, and slippery gravel in fast-flowing headwaters and minor tributaries. Bioinspired by the adhesion characteristics, two-dimensional non-close-packed colloidal crystals are self-assembled and serve as templates to pattern crescent-shaped shape memory polymer-based nanostructure arrays. By the manipulation of the configuration of nanosuckers through applying common solvent stimulations, the corresponding adhesion performances on glass, sandpaper, or even porcine kidney surfaces can be switched instantaneously and reversibly under ambient conditions. The biomimetic nanostructures indicate possible solutions to a variety of challenges, such as wound nursing, and so on.

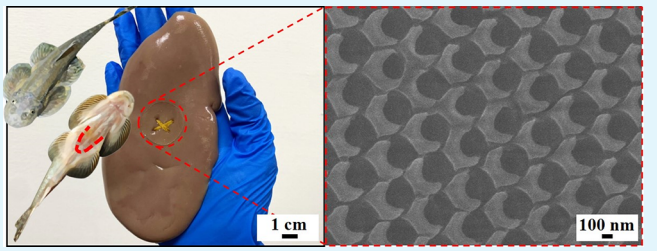

KEYWORDS: *Hemimyzon formosanus, adhesion, self-assembly, crescent-shaped nanosucker arrays, shape memory polymer*

INTRODUCTION

Over 3.6 billion years of natural selection and evolution, living creatures have developed versatile strategies to address diverse survival challenges. By way of illustration, insects and spiders use curved grapnel-like claws and dense tufts of fine bristles on cuticular surfaces to climb and promote attachments through interlocking with rough surfaces.[1−3] Instead of microharis, the hierarchical structures of setae and spatulae on gecko feet generate van der Waals forces as they are in intimate contact with a target.[4,5] By applying anisotropic directional stresses onto their spatulae, geckos can rapidly switch and control their adhesion strengths for locomotion onto vertical or even inverted surfaces. In sharp contrast to the dry adhesion mechanism, mussels secrete specialized proteins, known as catecholic amino 3, 4-dihydroxyl-L-phenylalanine (DOPA), for clinging to wet surfaces.[6,7] The DOPA and its derivatives have demonstrated extraordinarily strong interfacial adhesions as a natural adhesive. Inspired by these biological adhesion mechanisms, numerous artificial architectures and adhesive materials with switchable adhesion performances have been reported.[8−14] The biomimetic materials have potential applications in smart-printing systems, industrial assembly and manipulation systems, and medical adhesives. However, it remains an enormous challenge to allow the insect-inspired microstructures to interlock with flat surfaces, while the gecko-inspired hierarchical structures suffer from complex manufacturing processes and poor mechanical properties. In addition, their adhesion abilities fail in wet environments. Although mussel-inspired adhesives can address the above-mentioned issues effectively, the adhesives are limited by low on/off adhesive strength ratios. Therefore, it is still in high demand to actively control the adhesion behaviors on both dry and wet surfaces.

Cephalopod arms are with non-close-packed bowl-like suckers along their entire ventral surfaces, allowing cephalopods to grasp free-swimming prey, to negotiate coral reefs with ease, and to anchor themselves on any foreign surface.[15,16] The suckers consist of the infundibulum and acetabulum regions, all of which are composites of different muscular structures. Once in contact with a target regardless of the surface materials, the infundibulum can be bent and conform to the surface, during which the ridges on the rim facilitate the formation of a watertight seal. The acetabulum then contracts radially to reduce the pressure inside the sucker cavity, thereby generating a pressure differential for suction on the target. The subambient pressure within the sucker can be maintained without any muscular activity for a long-term attachment. During detachment, the contraction of circular muscles in the infundibulum ruptures the seal, making the internal sucker pressure equivalent to that of the surrounding environment. Bioinspired by the adhesion mechanism, numerous artificial cephalopod suckers have been developed to achieve switchable adhesion capabilities in dry and underwater environ-

Received: October 18, 2023
Revised: November 12, 2023
Accepted: November 14, 2023
Published: November 27, 2023

ments.[17−23] Nevertheless, these cephalopod-inspired adhesion systems can only be applied on flat targets, whereas the systems cannot form seals on rough surfaces, to say nothing of attaching to them. The requirement of sufficient power sources or external mechanical forces in the attachment and detachment processes is another inherent issue that needs to be addressed.[24,25] Moreover, it remains a great challenge to control their switchable adhesion properties immediately as required.[26,27]

Hemimyzon formosanus, a genus of ray-finned fish in the family Balitoridae, lives in clear and well-oxygenated torrents of Taiwan's Central Mountain Range.[28,29] Instead of circular suckers, they have crescent-shaped ventral fins for clinging to slippery gravels with jumbles of boulders. Although the crescent-shaped structures allow them to switch the adhesion behaviors instantly on demand, the related artificial suckers have rarely been reported.[30] Furthermore, there is a practical difficulty in the formation of crescent-shaped suckers and maintaining their attachments for a long period of time.

Stimuli-responsive materials, which can reversibly switch their configurations in response to external stimuli, facilitate the invention of reconfigurable micro- and nanoscale features.[31,32] Even though the reconfigurable structures provide a facile strategy to achieve tunable adhesion characteristics, most of their intermediate structures cannot be preserved when the driving forces are removed. Over the years, the discovery of diverse shape memory polymers (SMP) renders a promising pathway to address this drawback of transient intermediate states.[33,34] The SMP-based structures can turn into rubbery states and be mechanically deformed above their glass-transition temperatures. Once the deformed structures are cooled below the transition temperatures, their temporary shapes become rigid and are fixed in the glassy states. Importantly, entropy-driven elastic recoveries occur as external stimuli, such as electric fields, ultraviolet radiations, and heat, are introduced to enhance polymer chain mobilities and to make the temporarily deformable structures to be reconstructed.[35] Unfortunately, most of the physical stimuli-responsive structural transitions are limited by fairly long durations, which severely hinder their practical applications. In comparison, it takes less time for chemical stimuli-induced structural recoveries.[36,37] However, these shape memory cycles still suffer from short-term operations. Furthermore, the adoption of specific organic solvents inevitably incurs adverse health issues and possesses detrimental impacts on other device components.

In sharp contrast to thermoresponsive SMPs, nontraditional polymers with all-room-temperature shape memory effects have been developed in the past years.[38,39] Their configurations can be immediately switched by controlling the evaporation of varied household solvents under ambient conditions. Herein, a room-temperature SMP is synthesized and introduced to engineer crescent-shaped nanostructure arrays by integrating a colloidal assembly technology and a templating fabrication methodology in this study. By characterizing the adhesion performances of Hemimyzon formosanus-inspired nanosucker arrays onto a diversity of targets, this research develops a better understanding of their switchable adhesion mechanisms. The findings undoubtedly provide a facile strategy to overcome the aforementioned challenges and to guide a wealth of emerging intelligent applications.

EXPERIMENTAL SECTION

Chemicals and Substrates. The reagents applied for spherical StÖber silica colloid synthesis, including absolute ethanol (≥99.8%), tetraethyl orthosilicate (≥99.5%), and ammonium hydroxide (≥23.8%), are provided by Merck KGaA. Ultrapure water with a resistivity of 18.2 MΩ·cm is supplied by a MilliporeSigma Milli-Q Direct 7 water purification system. Ethoxylated trimethylolpropane triacrylate (ETPTA, SR 454) monomers, ethylene glycol diacrylate (EGDA, SR 610) monomers, and 2-hydroxy-2-methyl-1-phenyl-1-propanone (HMPP, Darocur 1173) as an initiator are acquired from Sartomer and BASF, respectively. Poly(vinyl alcohol) (PVA, M_w 89,000−98,000, ≥ 99.0%) is obtained from Merck KGaA. (Tridecafluoro-1, 1, 2, 2-tetrahydroocity)trichlorosilane (≥97.0%), purchased from Alfa Aesar, is used as a surface modifier. All of the above chemicals are of reagent quality and utilized directly in this study. Commercial silicon wafers (test grade, n-type (100), Wafernet), are rinsed with ultrapure water and then primed by 3-acryloxypropyl trichlorosilane (APTCS, ≥ 96.0%, Gelest) before use. In the APTCS-priming process, APTCS-overlaid wafers are rinsed with absolute ethanol at 2000 rpm for 2 min on a WS-400B-6NPP-Lite spin-coater (Laurell) and baked at 105 °C for 30 s afterward.

Fabrication of Monolayer Non-Close-Packed Colloidal Crystals. Non-close-packed silica colloidal crystals are self-assembled according to a well-established spin-coating technology.[40,41] Spherical StÖber silica colloids with an average diameter of 250 nm are purified in absolute ethanol to remove unreacted chemicals through multiple centrifugation/redispersion cycles, followed by redispersing in UV-curable ETPTA monomers with 1 vol % of HMPP as the photoinitiator.[42] The volume fraction of silica colloids with respect to ETPTA monomers in the colloidal suspension is adjusted to be 1:4. After any colloid aggregate was eliminated by filtering the suspension through a 1.2 μm syringe filter, the silica colloidal suspension is deposited and spread onto an APTCS-primed silicon wafer. The wafer is then transferred into a standard spin-coater and spun at 1000 rpm for 2.5 min, 3000 rpm for 2 min, 5000 rpm for 1.5 min, and 7000 rpm for 3 min, progressively, to shear-align silica colloids. The ETPTA monomers are finally photopolymerized on exposure to UV-radiation in an X-Lite-500 UV curing chamber (OPAS).

Preparation of Nanohole Arrays. The embedded silica colloids are partially released through argon reactive-ion etching (RIE) the as-assembled non-close-packed silica colloidal crystal/poly(ETPTA) composite on a Shuttlelock-770 inductively coupled plasma processing system (Orelikon). The RIE process is performed with ultrapure argon gas at a flow rate of 40 sccm for 50 s, while the chamber pressure and power density are kept at 40 mTorr and 100 W, respectively. Subsequently, a PVA aqueous solution (5 vol %) is poured onto the plasma-etched composite and then dried at room temperature. The resulting monolayer silica colloidal crystal-embedded PVA film can be peeled off from the wafer. Upon stretching unidirectionally, the PVA matrix is deformed to create a non-close-packed crescent-shaped nanohole array.

Templating Fabrication of Crescent-Shaped Nanosucker Arrays. The surface energy of the silica colloidal crystal-embedded PVA nanohole array is further reduced through surface functionalization with fluorosilanes in a chemical vapor deposition process. During the surface modification, the PVA substrate and a beaker of (tridecafluoro-1, 1, 2, 2-tetrahydrooctyl)trichlorosilane are placed in a vacuum oven. The oven can be evacuated with a vacuum pump to allow volatilized fluorosilanes to react with the hydroxyl groups of silica colloids and PVA macromolecules at 70 °C. After 45 min, the PVA substrate is transferred into a vacuum chamber for eliminating any physically adsorbed fluorosilane. A mixture of ETPTA monomers (24 vol %), EGDA monomers (75 vol %), and HMPP (1 vol %) is well-mixed and then poured over the surface-modified PVA nanohole array gently. After a degassing process, the UV-curable monomer mixture is photopolymerized under UV-radiation. Afterward, the as-synthesized poly(ETPTA)/poly(EGDA) copolymer can be peeled off from the unidirectionally stretched PVA template to bring about a crescent-shaped nanosucker array.

https://doi.org/10.1021/acsami.3c15577
ACS Appl. Mater. Interfaces 2023, 15, 56203−56212

Characterization. Photographic and scanning electron microscopy (SEM) images are obtained using an EOS R10 digital camera (Canon) and a 6335F FEG-SEM (JEOL), respectively. The specimens are sputter-coated with a gold layer on a 108auto sputter coater (Cressington) prior to SEM imaging. Optical microscopy images are acquired from a DM4 optical microscope (Leica). Adhesion force characteristics of the specimens are determined by a NK-20 mechanical force gauge (Algol Instrument) and an EZ test table-top universal testing instrument (Shimadzu). The specimens are pressed against a glass slide, followed by tensile pulling-off from the glass substrate along the normal direction. The tensile-adhesion measurements of each specimen are repeated 10 times, and the average values are reported.

RESULTS AND DISCUSSION

Bioinspired by the adhesion characteristics of Hemimyzon formosanus, crescent-shaped nanosucker arrays are designed and built through integration of a scalable colloidal self-assembly technology and a soft-lithography-like process. As presented in Figure 1, a silica colloidal monolayer/poly-

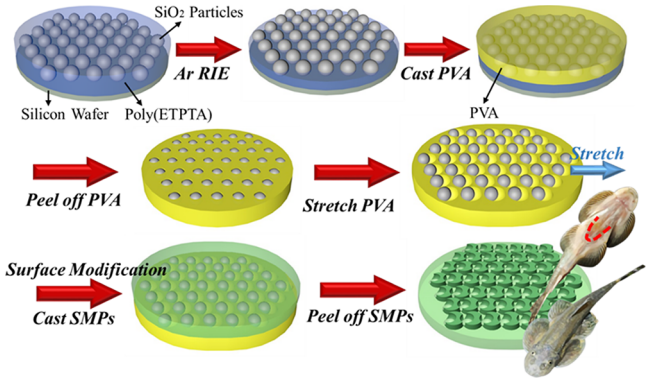

Figure 1. Schematic illustration of the experimental procedures for engineering crescent-shaped nanosucker arrays.

(ETPTA) composite is spin-coated onto an APTCS-primed silicon wafer, during which the colloids are self-assembled into a hexagonally non-close-packed arrangement. On account of the high RIE selectivity between silica colloids and poly(ETPTA) macromolecules, the embedded silica colloidal crystals are released under an argon plasma etching. Subsequently, a PVA aqueous solution is cast upon the plasma-treated composite and then dried under ambient conditions. The resulting monolayer silica colloidal crystal-embedded PVA film can be peeled off from the silicon wafer. Upon stretching unidirectionally, the PVA matrix is deformed to bring about a non-close-packed crescent-shaped nanohole array. After surface modification, the PVA templates are cast with a mixture of ETPTA monomers, EGDA monomers, and HMPP, followed by a degassing process to eliminate any trapped air. The UV-curable monomer mixture is finally photopolymerized and peeled off from the surface-modified templates to create crescent-shaped poly(ETPTA)/poly(EGDA) copolymer nanosuckers. Even though the fabrication procedures are relatively complicated, the surface-functionalized PVA templates can be well-preserved after the templating fabrication process, and reused to bring about nanosucker arrays.[43]

Here, a 4 in. wafer-scale 250 nm silica colloidal crystals is realized through spin-coating a concentrated silica colloidal suspension onto a silicon wafer. In the shear-aligning process, the wafer edges possess higher rotational velocities; hence the silica colloids in the edge region are provided with stronger shear-moments, and are stripped away earlier from the wafer.[44,45] The resulting vacancies are subsequently filled with neighboring silica colloids, leading to the formation of nonuniform shear flows along radial directions and a pressure gradient exerted normal to the wafer surface. The normal pressure further squeezes the hexagonally arranged silica colloidal layers into each other, bringing about the unusual non-close-packing arrangement. In addition to the silicon substrate, non-close-packed hexagonal colloidal crystals can be shear-aligned on various polymer and glass substrates.[46,47] The as-assembled monolayer silica colloidal crystal/poly(ETPTA) composite displays a distinctive six-arm pattern under white light illumination (Figure 2a), resulting from the Bragg

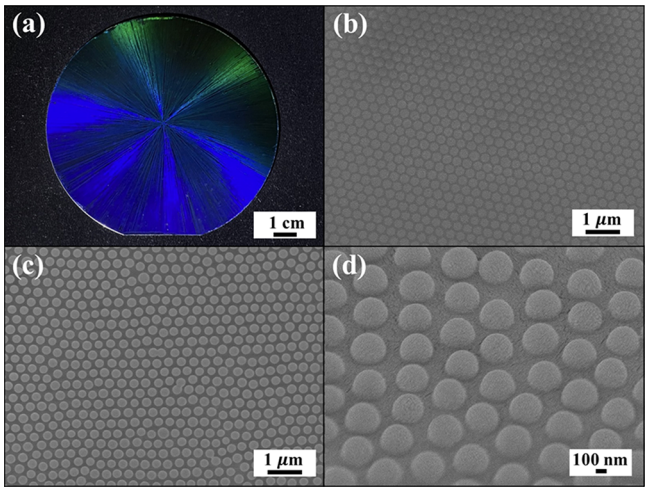

Figure 2. (a) Photographic image and (b) top-view SEM image of a non-close-packed 250 nm silica colloidal crystal/poly(ETPTA) composite spin-coated on a silicon wafer. (c) Top-view SEM image and (d) magnified tilted-view SEM image of the composite treated with an argon reactive ion etching.

diffraction of hexagonally non-close-packed colloidal crystals.[48] The long-range crystal lattice is further evidenced from its top-view SEM image (Figure 2b). Importantly, the embedded silica colloids can be partially released by performing an argon RIE treatment (Figure 2c,d), during which the silica colloids serve as etching masks to prevent the poly(ETPTA) matrix underneath from being etched. As a result, a non-close-packed hemispherical silica protrusion array is created. The average intercolloid distance equals to approximate $\sqrt{2}D$, where D refers to the diameter of silica colloids. It is worthy to note that the intercolloid distance is identical to those of shear-aligned colloidal crystals composed of submicrometer-sized particles, evincing a similar self-assembly mechanism for the colloidal crystallization process.[44−49] On account of the hydrogen bonding between silica colloids and PVA macromolecules, the silica colloidal crystals can be easily transferred and evenly embedded onto a PVA substrate (Figure S1). It is clear that the long-range hexagonal ordering and non-close-packed arrangement of silica colloids are well-preserved, leading to the presentation of another six-arm pattern.

The silica colloidal crystal-embedded PVA films can be stretched unidirectionally to generate crescent-shaped nanohole arrays (Figure 3). Apparently, the nanoholes are getting larger with the increase of the uniaxial elongation ratio. After

https://doi.org/10.1021/acsami.3c15577
ACS Appl. Mater. Interfaces 2023, 15, 56203−56212

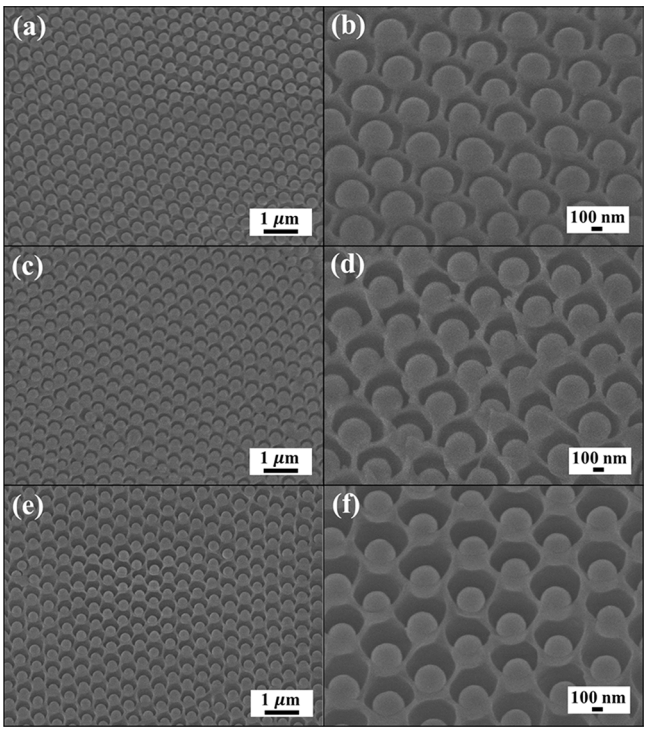

Figure 3. Top-view SEM images of 250 nm silica colloidal crystal-embedded PVA composite films under varied elongation ratios of (a, b) 10%, (c, d) 20%, and (e, f) 30%. The PVA films are stretched unidirectionally.

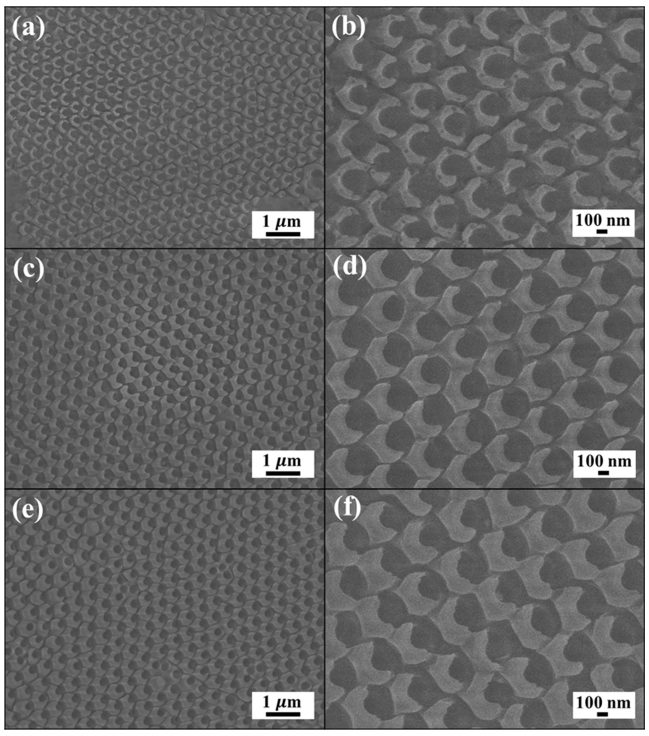

Figure 4. Top-view SEM images of crescent-shaped poly(ETPTA)/poly(EGDA) copolymer nanosucker arrays templated from unidirectionally stretched PVA composite films. The elongation ratios of the PVA composite films are (a, b) 10%, (c, d) 20%, and (e, f) 30%, respectively.

surface functionalization with fluorosilanes to reduce their surface energies, the PVA films are utilized as second-generation templates to pattern poly(ETPTA)/poly(EGDA) copolymer nanosucker arrays. Interestingly enough, nanometer-scale old moon-shaped structures (Figure 4a,b), waxing crescent-shaped structures (Figure 4c,d), and waxing quarter-shaped structures (Figure 4e,f) are therefore engineered, respectively, as the elongation ratio of PVA templates varies from 10, 20, to 30%. Although the interstructure distances and long-range hexagonal orderings are well-retained during the templating process, their structure sizes are slightly reduced by ~3% than expected. The results are primarily caused by the volume shrinkage of PVA matrices in the photopolymerization procedure, during which the entrapped water is evaporated on exposure to UV-radiation. Importantly, it is evident that non-close-packed nanoconcaves (dark areas of the SEM images), surrounded by disconnected nanometer-scale crescent-shaped structures, are also templated from the embedded silica colloids.

The combination of nanometer-scale crescent-shaped structures and nanoconcreta can function as nanosuckers (Figure 5a). Poly(ETPTA)/poly(EGDA) copolymers exhibit distinctive shape memory characteristics, which allow their configurations to be altered in response to external stimuli under ambient conditions. Upon rinsing with water, the penetration of water molecules into the shape memory polymer (SMP) network leads to a volume increase, while the spacing between crescent-shaped structures is reduced accordingly. The swollen structure array can conform to a target of choice for building up enclosed spaces, and then be deformed to release entrapped air within the enclosures as the flexible structure array is pressed against the target surface (Figure S2). It is evidenced that a higher pressure applied onto

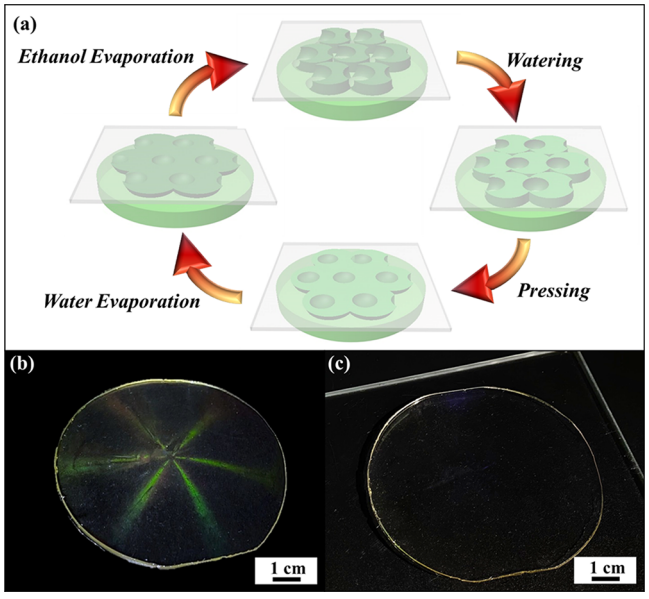

Figure 5. (a) Schematic illustration of the attachment and detachment mechanisms. (b) Photographic image of a 4-in. wafer-scale crescent-shaped SMP nanosucker array illuminated with white light. The elongation ratio of unidirectionally stretched PVA templates is controlled to be 20%. (c) Photographic image of the same specimen as in (b) adhering to a glass substrate.

the structures leads to the formation of smaller enclosures, and the structures are fully deformed as the pressure reaches 1 kPa. Subsequently, the fully deformed structures are dried under ambient conditions, during which a pressure of 1 kPa is applied

https://doi.org/10.1021/acsami.3c15577
ACS Appl. Mater. Interfaces 2023, 15, 56203−56212

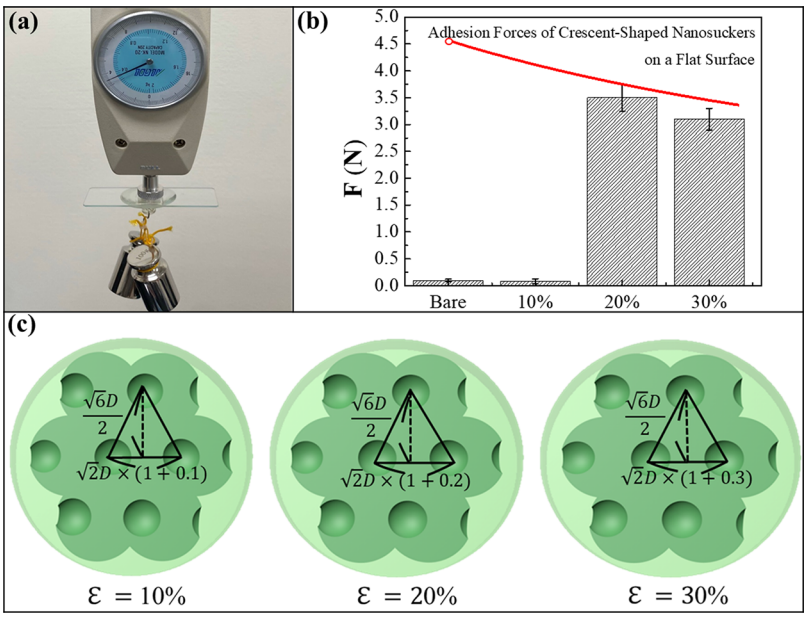

Figure 6. (a) Adhesion force measurement of a 1 cm^2-sized crescent-shaped SMP nanosucker array performed using a tension gauge. The structures are templated from a unidirectionally stretched PVA composite film with an elongation ratio of 20%. (b) Adhesion forces of a 1 cm^2-sized featureless SMP film and 1 cm^2-sized crescent-shaped SMP nanosucker arrays templated from unidirectionally stretched PVA composite films with varied elongation ratios of 10, 20, and 30%. (c) Illustration of the crescent-shaped SMP nanosucker arrays.

to maintain their deformed configurations. After drying out of water in a few minutes, the deformed enclosures can be well-preserved to bring about a low-pressure cavity array. The corresponding pressure difference between surrounding atmospheric environments and the cavities thereupon generates an adhesion force to keep the nanosuckers adhered to the target. Instead of physical forces, the temporarily deformed crescent-shaped structures recover their permanent configurations through drying out of ethanol. Once rinsing with ethanol, the absorbed ethanol molecules can relax the compressed copolymer chains, and hence enhance their mobilities. The dominancy of ethanol evaporation-induced capillary pressure over the copolymer entropy elasticity further drives the squeezed structures to recover their original conformations.[50,51] In other words, the external energy is employed to overcome the shape memory activation barrier and thus to trigger the shape recovery. On account of the structural recovery, air is permitted to leak back into the crescent-shaped structures; thereafter, the reduced pressure difference results in the detachment of nanosuckers. As shown in Figure 5b, a 4-in. non-close-packed crescent-shaped SMP nanosucker array, templated from a unidirectionally stretched silica colloidal crystal-embedded PVA film, exhibits a characteristic six-arm star pattern under white light illumination. The adjacent arms form exact 60° angles, indicating the presence of hexagonally arranged nanosucker array.[44,48] This pattern further shows evidence of its wafer-scale periodic domain ordering. In comparison with that, the same specimen adhering to a glass substrate becomes highly transparent in appearance (Figure 5c). The results disclose that the nanosuckers are fully deformed, and thereby incident visible light is not diffracted from them. Even though the color of the diffraction star changes with its viewing angle, the adhesion behaviors of the SMP nanosucker array can be sketchily determined by the six-arm pattern transformation.

The adhesion capacities of crescent-shaped SMP nanosucker arrays on flat microscope slides are evaluated by using a tension gauge and a table-top universal testing instrument. As compared in Figure 6a,b, it is found that a bare SMP film (1 cm^2 in size) displays an adhesion force of less than 0.1 N, which mainly results from the van der Waals forces at the polymer/glass interface. Surprisingly, the adhesion capability of the SMP nanosucker array, templated from a unidirectionally stretched PVA composite film with an elongation ratio of 10%, is enhanced slightly. It is believed that the old moon-shaped structures are with slimmer conformations and larger spaces in between (Figure 4a,b). As a result, the swollen old moon-shaped structures cannot form seals much less adhere to the glass slide. In sharp contrast, the average adhesion forces of waxing crescent-shaped SMP structures (Figure 4c,d) and waxing quarter-shaped SMP structures (Figure 4e,f), templated from unidirectionally stretched PVA templates with elongation ratios of 20 and 30%, can reach 3.5 and 3.2 N per square centimeter, respectively. Importantly, the nanosuckers can be deformed and adhere to the target under an extremely low preload (Figure S3). Compared with that, the recorded force increases greatly during the structural recovery. An apparent adhesion force, mainly caused by the pressure difference between the surrounding atmosphere and the cavities, is evident in the pull-off process. The further structural deformation results in more conformal interactions between the polymers, and thus a larger pull-off force at the break-off point. Their adhesion capabilities are even competitive with commercial polymer-based dry adhesives.[52−54] To gain a better understanding, theoretical adhesion forces of the crescent-shaped SMP nanosucker arrays (1 cm^2 in size) are estimated by the following equation:

$$F_{\text{adhesion}} = \Delta P \times A \times N_{\text{total}} \quad (1)$$

where ΔP represents the difference between atmospheric pressure and the pressure within the nanosuckers; A refers to the area of attachment for each nanosucker; and N_{total} denotes the number of nanosuckers in contact with a flat target surface. Assuming that the air enclosed within the structures is

https://doi.org/10.1021/acsami.3c15577
ACS Appl. Mater. Interfaces 2023, 15, 56203−56212

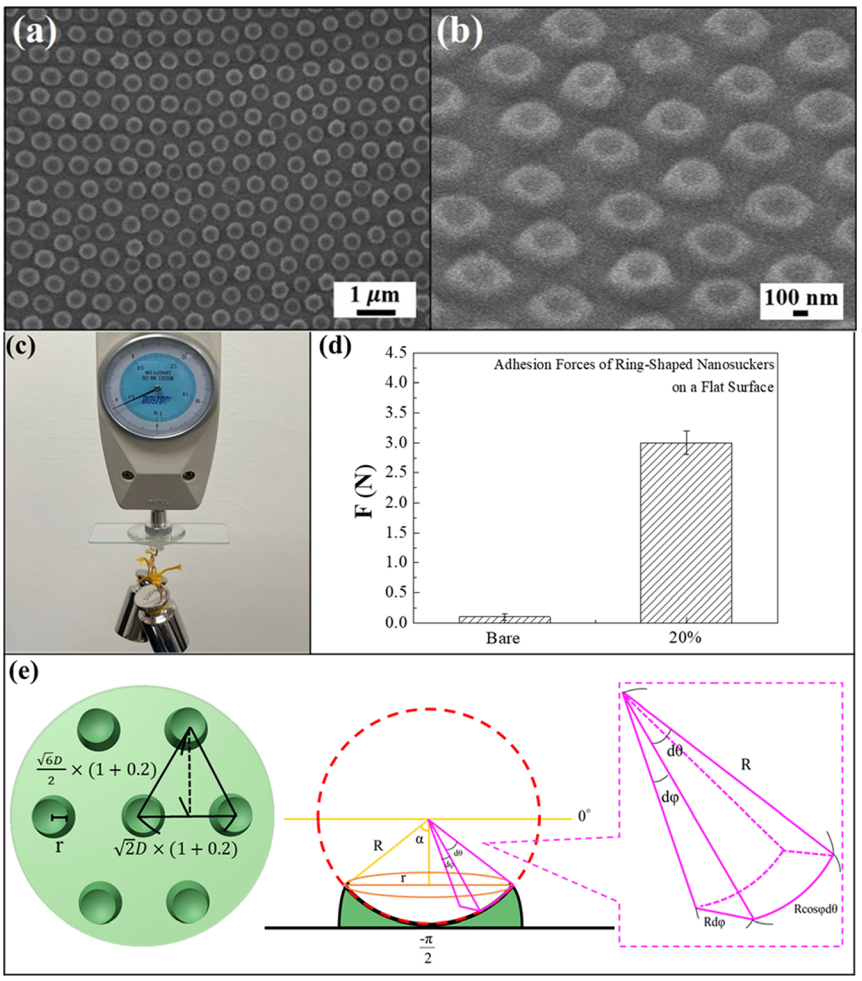

Figure 7. (a) Top-view SEM image and (b) magnified tilted-view SEM image of a ring-shaped SMP nanosucker array templated from a biaxially stretched PVA composite film. The elongation ratio of the PVA composite film is 20%. (c, d) Adhesion force of the ring-shaped SMP nanosucker array (1 cm^2 in size). (e) Illustration of a ring-shaped SMP nanosucker.

completely released, ΔP is given by the value of 10.1 N/cm^2. In that case, A equals to $\frac{\pi D^2}{2}$, where D is the diameter of templating silica colloids. As illustrated in Figure 6c, the internanosucker distance in the stretching direction increases linearly with the elongation ratio (ε), whereas the distance remains unchanged in the perpendicular direction. Accordingly, the total number of nanosucker on a 1 cm^2 SMP specimen can be expressed by $N_{total} = \frac{1\ cm^2}{\sqrt{3}(1+\varepsilon)D^2}$. As a result, $F_{adhesion}$, which is much larger than van der Waals forces, is decreased with the increase of ε (red curve in Figure 6b). It is worth mentioning that the theoretical adhesion forces and measured values display similar evolution trends. The results confirm that the crescent-shaped SMP structures are capable of sustaining negative pressures.

The adhesion capacity difference between crescent-shaped and ring-shaped nanosuckers is further investigated in this study. Instead of unidirectional stretching, the silica colloidal crystal-embedded PVA film is stretched biaxially to create ring-shaped nanoholes (Figure S4). Its elongation ratios along both stretching directions are controlled to be 20%. As shown in Figure S5, the long-range hexagonally non-close-packed arrangement of nanoholes is clearly evidenced. After surface modification, the nanohole array is utilized to pattern a ring-shaped SMP nanosucker array (Figure 7a,b). Compared with the adhesion force of crescent-shaped nanosuckers, the ring-shaped nanosuckers exhibit a similar adhesion capability of 3.0 N per square centimeter on a flat substrate (Figure 7c,d), which can also be theoretically estimated using eq 1. For a 1 cm^2-sized specimen, the total number of nanosucker (N_{total}) is expressed in terms of $\frac{1\ cm^2}{\sqrt{3}(1+\varepsilon)^2D^2}$ (Figure 7e), while the area of attachment for each nanosucker can be appraised as follows.

$$A = \int_0^{2\pi} \int_{-\pi/2}^{\alpha-\pi/2} R^2 \cos\varphi \, d\varphi \, d\theta \quad (2)$$

In the above equation, $\varphi = \frac{\pi}{2} - \alpha$, and $R \sin\alpha = r$, where R and r denote the radii of templating silica colloids and nanosucker opening, respectively. It is recognized that $r \approx 100$ nm (Figure 7b), thereby α (~53.1°) and φ (~36.9°) can be calculated. After the φ and R are inputting into eq 2 to compute A, the A and N_{total} in eq 1 are substituted to determine the $F_{adhesion}$ of the ring-shaped nanosucker array. Apparently, the theoretical adhesion force (2.9 N per square centimeter) agrees well with the measured one (3.0 N per square centimeter). It is worth noting that the adhesion force difference shall be attributed to van der Waals forces between the nanostructures and the target surface.

To comprehend their adhesion performances, the adhesion strengths of a 1 cm^2-sized waxing crescent-shaped SMP

https://doi.org/10.1021/acsami.3c15577
ACS Appl. Mater. Interfaces 2023, 15, 56203−56212

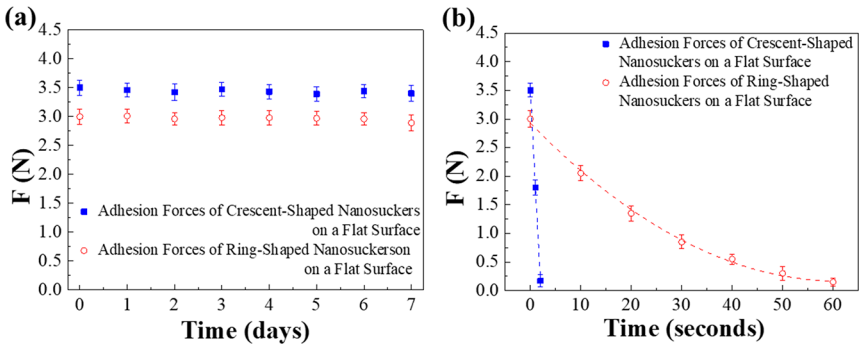

Figure 8. (a) Adhesion force changes of a 1 cm^2-sized crescent-shaped SMP nanosucker array and a 1 cm^2-sized ring-shaped SMP nanosucker array over time. (b) Adhesion force changes of the SMP nanosucker arrays over time in the detachment process.

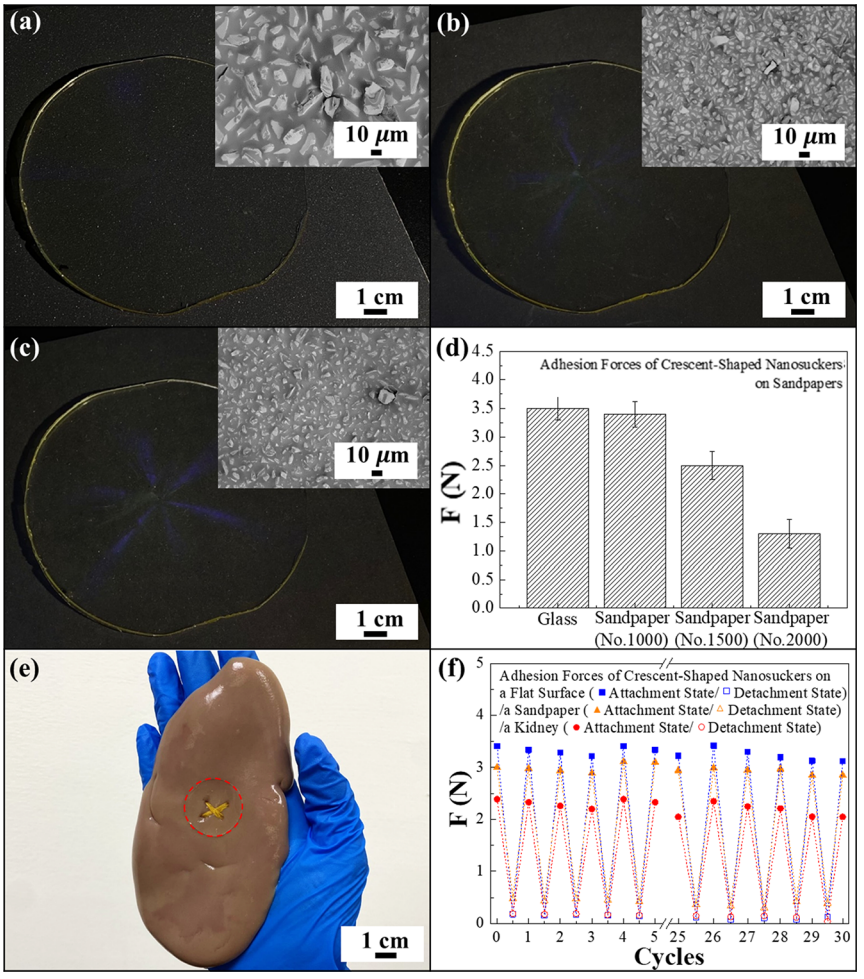

Figure 9. Photographic images of crescent-shaped SMP nanosucker arrays adhering to (a) a 1000-grit sandpaper, (b) a 1500-grit sandpaper, and (c) a 2000-grit sandpaper. The insets show top-view SEM images of the sandpapers. The structure arrays are templated from a unidirectionally stretched PVA composite film with an elongation ratio of 20%. (d) Adhesion forces of 1 cm^2-sized crescent-shaped SMP nanosucker arrays on varied sandpapers. (e) Photographic image of the nanosucker array adhering to a porcine (pig) kidney. (f) Adhesion forces of the nanosucker arrays on a glass substrate, a 1000-grit sandpaper, and a porcine kidney after 30 attachment/detachment cycles.

nanosucker array and a 1 cm^2-sized ring-shaped SMP nanosucker array over time are evaluated. It is found that both SMP nanosucker arrays are capable of maintaining stable attachments for more than 1 week (Figure 8a). Once rinsing with ethanol, the temporarily deformed nanosuckers can gradually recover their original configurations as the ethanol evaporates in ambient conditions. The resulting shape recovery allows air to leak back into the nanoconcave, bringing about decreased pressure differentials and reduced adhesion strengths with time (Figure 8 b). It is noticed that the adhesion force of ring-shaped nanosuckers is gradually diminished within 1 min. In contrast, the adhesion strength of waxing crescent-shaped nanosuckers is vanished in 2 s, indicating that the detachment can be realized instantaneously. To put is simply, the presence of crescent-shaped structures provides a facile manner to impede the sealings on demand,

https://doi.org/10.1021/acsami.3c15577
ACS Appl. Mater. Interfaces 2023, 15, 56203−56212

and thus it takes much shorter for detachment. Importantly, preloads are not required for the crescent-shaped nanosuckers during the detaching procedure, which is promising for diverse advanced materials and technological applications. Although thermoresponsive shape memory polymers have been utilized in making tunable three-dimensional structures, which can realize their shape memory transitions within a few minutes, the heat-demanding shape memory programming and recovery steps considerably impede the ultimate performance and applications.[55−58]

In addition to flat targets, the Hemimyzon formosanus-inspired nanosuckers are capable of adhering to microrough surfaces. To investigate this feasibility, the adhesion performances of a waxing crescent-shaped nanosucker array on 1000-grit, 1500-grit, and 2000-grit sandpapers are evaluated. As displayed in Figure 9a, the appearance of crescent-shaped nanostructure-patterned SMP film turns transparent once the specimen adheres to a piece of 1000-grit sandpaper. This finding discloses that most of the nanosuckers can be fully deformed and release the entrapped air within the enclosures onto tens of micrometer-sized abrasive grains on which an adhesion force is therefore generated. In comparison with that, the specimen attached to a micrometer-sized abrasive grain-covered sandpaper presents a blurred six-arm pattern (Figure 9b). Interestingly, the pattern becomes even clearer as a submicrometer-sized abrasive grain-covered sandpaper serves as a target (Figure 9c). Although the bioinspired nanosuckers can attach to both flat and microrough surfaces, less nanosuckers are in direct contact with smaller abrasive grains, while relatively poorer sealing properties are performed. As a result, adhesion strengths are reduced on rougher surfaces (Figure 9d). To further verify that, their adhesion strengths on varied sandpaper-roughened glass surfaces are evaluated (Figure S6). The glass substrates are abraded with 1000-grit, 1500-grit, and 2000-grit sandpapers for 100 cycles of abrasion under a normal loading of 12.5 kPa. Clearly, the nanosucker arrays exhibit similar tendencies on both sandpaper and sandpaper-roughened glass substrates. In spite of that, it is believed that the adhesion strength can be considerably enhanced by introducing smaller nanosuckers. The adhesion performance of waxing crescent-shaped SMP nanosuckers on a porcine kidney is also presented as a proof-of-concept demonstration to assess their adhesion capability on wet surfaces in this study (Figure 9e). Apparently, the specimen can attach to the wet microrough organ surface and turns optically transparent under natural light illumination, where the yellow sutures underneath are clearly observed. The pellucid film dressings provide a platform for real-time inspection on wound healing and noncompressible hemostasis. It is significant to mention that the SMP structures can be reversibly deformed and recovered in response to external stimuli, which realizes switchable attachment/detachment functionalities. As verified in Figure 9f, the Hemimyzon formosanus-inspired adhesion can be repeatedly applied on glass, 1000-grit sandpaper, and kidney surfaces for at least 30 attachment/detachment cycles in the ambient environment. Although the adhesion strengths are slightly reduced over multiple contact cycles, caused by the deformation of waxing crescent-shaped structures in the attachment process, most structures are well-retained after 30 shape memory cycles (Figure S7).

CONCLUSIONS

To conclude, stimuli-responsive shape memory polymer-based crescent-shaped nanosucker arrays are developed by integrating a scalable colloidal self-assembly technology and an uncomplicated templating methodology. The as-engineered structure arrays can be deformed and generate long-term adhesion strengths onto flat, microrough, or even biological surfaces. Instead of physical forces, the temporarily deformed crescent-shaped structures recover their original configurations through drying out of ethanol, resulting in vanished adhesion strengths in a few seconds. The reversible structural transition realizes switchable attachment/detachment functionalities and creates novel dimensions for a diversity of household supplies, medical applications, and semiconductor manufacturing.

ASSOCIATED CONTENT

Supporting Information

The Supporting Information is available free of charge at https://pubs.acs.org/doi/10.1021/acsami.3c15577.

Photographic images and SEM images of silica colloidal crystal/PVA composites and crescent-shaped nanosucker arrays; adhesion force−displacement curve of a crescent-shaped nanosucker array; schematic illustration of the experimental procedures for engineering ring-shaped nanosucker arrays; and adhesion forces of crescent-shaped nanosucker arrays on varied sandpaper-roughened glass substrates (PDF)

AUTHOR INFORMATION

Corresponding Author

Hongta Yang − *Department of Chemical Engineering, National Chung Hsing University, Taichung 40227, Taiwan;* orcid.org/0000-0002-5822-1469; Email: hyang@dragon.nchu.edu.tw

Authors

Jung-Hsuan Hsu − *Department of Chemical Engineering, National Chung Hsing University, Taichung 40227, Taiwan*

Nien-Ting Tang − *Department of Chemical Engineering, National Chung Hsing University, Taichung 40227, Taiwan*

Ting-Fang Hsu − *Department of Chemical Engineering, National Chung Hsing University, Taichung 40227, Taiwan*

Shin-Hua Lin − *Department of Chemical Engineering, National Chung Hsing University, Taichung 40227, Taiwan*

Cai-Yin Fang − *Department of Chemical Engineering, National Chung Hsing University, Taichung 40227, Taiwan*

Yun-Wen Huang − *Department of Chemical Engineering, National Chung Hsing University, Taichung 40227, Taiwan*

Complete contact information is available at: https://pubs.acs.org/10.1021/acsami.3c15577

Author Contributions

†J.-H. H. and N.-T. T. contributed equally.

Notes

The authors declare no competing financial interest.

ACKNOWLEDGMENTS

The acknowledgments are made to the Instrument Center of National Chung Hsing University for the technical support with the scanning electron microscope. This research was financially supported by the National Science and Technology

Council (MOST 110-2221-E-005-050-MY2, MOST 111-2221-E-005-010, and NSTC 112-2221-E-005-006-MY3) and the Innovative Center on Sustainable Negative-Carbon Resources from The Featured Areas Research Center Program within the framework of the Higher Education Sprout Project by the Ministry of Education.

REFERENCES

(1) Feat, A.; Federle, W.; Kamperman, M.; van der Gucht, J. Coatings Preventing Insect Adhesion: An Overview. *Prog. Org. Coat.* **2019**, *134*, 349−359.
(2) Recla, L.; Rheault, M.; Golovin, K. Complete Inhibition of Vertical Mosquito Landing through Topographical Surface Design. *ACS Appl. Mater. Interfaces* **2022**, *14* (33), 38320−38327.
(3) Tadayon, M.; Younes-Metzler, O.; Shelef, Y.; Zaslansky, P.; Rechels, A.; Berner, A.; Zolotoyabko, E.; Barth, F. G.; Fratzl, P.; Bar-On, B.; et al. Adaptations for Wear Resistance and Damage Resilience: Micromechanics of Spider Cuticular "Tools". *Adv. Funct. Mater.* **2020**, *30* (32), No. 2000400.
(4) Zhang, Y. L.; Ma, S. H.; Li, B.; Yu, B.; Lee, H.; Cai, M. R.; Gorb, S. N.; Zhou, F.; Liu, W. M. Gecko's Feet-Inspired Self-Peeling Switchable Dry/Wet Adhesive. *Chem. Mater.* **2021**, *33* (8), 2785−2795.
(5) Song, Y.; Wang, Z. Y.; Li, Y.; Dai, Z. D. Electrostatic Attraction Caused by Triboelectrification in Climbing Geckos. *Friction* **2022**, *10* (1), 44−53.
(6) Priemel, T.; Palia, R.; Babych, M.; Thibodeaux, C. J.; Bourgault, S.; Harrington, M. J. Compartmentalized Processing of Catechols During Mussel Byssus Fabrication Determines The Destiny of DOPA. *Proc. Natl. Acad. Sci. U. S. A.* **2020**, *117* (14), 7613−7621.
(7) Shin, M.; Shin, J. Y.; Kim, K.; Yang, B.; Han, J. W.; Kim, N. K.; Cha, H. J. The Position of Lysine Controls The Catechol-Mediated Surface Adhesion and Cohesion in Underwater Mussel Adhesion. *J. Colloid Interface Sci.* **2020**, *563*, 168−176.
(8) Tan, D.; Wang, X.; Liu, Q.; Shi, K.; Yang, B. S.; Liu, S.; Wu, Z. S.; Xue, L. J. Switchable Adhesion of Micropillar Adhesive on Rough Surfaces. *Small* **2019**, *15* (50), No. 1904248.
(9) Croll, A. B.; Hosseini, N.; Bartlett, M. D. Switchable Adhesives for Multifunctional Interfaces. *Adv. Mater. Technol.* **2019**, *4* (8), No. 1900193.
(10) Song, Y. G.; Hu, Y. L.; Zhang, Y. C.; Li, G. Q.; Wang, D. W.; Yang, Y.; Zhang, Y. F.; Zhang, Y. Y.; Zhu, W. L.; Li, J. W.; et al. Flexible Tri-switchable Wettability Surface for Versatile Droplet Manipulations. *ACS Appl. Mater. Interfaces* **2022**, *14* (32), 37248−37256.
(11) Fang, Y. L.; Xiong, X. H.; Yang, L.; Yang, W. Y.; Wang, H.; Wu, Q.; Liu, Q. W.; Cui, J. X. Phase Change Hydrogels for Bio-Inspired Adhesion and Energy Exchange Applications. *Adv. Funct. Mater.* **2023**, *33* (27), No. 2301505.
(12) Ma, S. H.; Wu, Y.; Zhou, F. Bioinspired Synthetic Wet Adhesives: From Permanent Bonding to Reversible Regulation. *Curr. Opin. Colloid Interface Sci.* **2020**, *47*, 84−98.
(13) Liu, Z. Y.; Yan, F. Switchable Adhesion: On-Demand Bonding and Debonding. *Adv. Sci.* **2022**, *9* (12), No. 2200264.
(14) Wang, Y. Z.; Lai, H.; Cheng, Z. J.; Zhang, H. Y.; Zhang, E. S.; Lv, T.; Liu, Y. Y.; Jiang, L. Gecko Toe Pads Inspired in Situ Switchable Superhydrophobic Shape Memory Adhesive Film. *Nanoscale* **2019**, *11* (18), 8984−8993.
(15) Tarazona, O. A.; Lopez, D. H.; Slota, L. A.; Cohn, M. J. Evolution of Limb Development in Cephalopod Mollusks. *eLife* **2019**, *8*, No. e43828.
(16) Wang, Z. H.; Zhu, X. W.; Cheng, X. X.; Bai, L. M.; Luo, X. S.; Xu, D. L.; Ding, J. W.; Wang, J. L.; Li, G. B.; Shao, P. H.; et al. Nanofiltration Membranes with Octopus Arm-Sucker Surface Morphology: Filtration Performance and Mechanism Investigation. *Environ. Sci. Technol.* **2021**, *55* (24), 16676−16686.
(17) Arzt, E.; Quan, H. C.; McMeeking, R. M.; Hensel, R. Functional Surface Microstructures Inspired by Nature - From Adhesion and Wetting Principles to Sustainable New Devices. *Prog. Mater. Sci.* **2021**, *120*, No. 100823.
(18) Liu, Q.; Meng, F. D.; Wang, X.; Yang, B. S.; Tan, D.; Li, Q.; Shi, Z. K.; Shi, K.; Chen, W. H.; Liu, S.; et al. Tree Frog-Inspired Micropillar Arrays with Nanopits on the Surface for Enhanced Adhesion under Wet Conditions. *ACS Appl. Mater. Interfaces* **2020**, *12* (16), 19116−19122.
(19) Fan, H. L.; Gong, J. P. Bioinspired Underwater Adhesives. *Adv. Mater.* **2021**, *33* (44), No. 2102983.
(20) Liang, Y. Q.; Xu, H. R.; Li, Z. L.; Zhangji, A. D.; Guo, B. L. Bioinspired Injectable Self-Healing Hydrogel Sealant with Fault-Tolerant and Repeated Thermo-Responsive Adhesion for Sutureless Post-Wound-Closure and Wound Healing. *Nano-Micro Lett.* **2022**, *14* (1), 185.
(21) Zhang, J.; Wang, Y. Y.; Zhang, J. J.; Lei, I. M.; Chen, G. D.; Xue, Y.; Liang, X. Y.; Wang, D. Z.; Wang, G. G.; He, S. S.; et al. Robust Hydrogel Adhesion by Harnessing Bioinspired Interfacial Mineralization. *Small* **2022**, *18* (31), No. 2201796.
(22) Yoo, J. I.; Kim, S. H.; Ko, H. C. Stick-and-Play System Based on Interfacial Adhesion Control Enhanced by Micro/Nanostructures. *Nano Res.* **2021**, *14* (9), 3143−3158.
(23) Bagheri, H.; Hu, A.; Cummings, S.; Roy, C.; Casleton, R.; Wan, A.; Erjavic, N.; Berman, S.; Peet, M. M.; Aukes, D. M.; et al. New Insights on the Control and Function of Octopus Suckers. *Adv. Intell. Syst.* **2020**, *2* (6), No. 1900154.
(24) Manabe, K.; Koyama, E.; Norikane, Y. Cephalopods-Inspired Rapid Self-Healing Nanoclay Composite Coatings with Oxygen Barrier and Super-Bubble-Phobic Properties. *ACS Appl. Mater. Interfaces* **2021**, *13* (30), 36341−36349.
(25) Choi, M. K.; Park, O. K.; Choi, C.; Qiao, S. T.; Ghaffari, R.; Kim, J.; Lee, D. J.; Kim, M.; Hyun, W.; Kim, S. J.; et al. Cephalopod-Inspired Miniaturized Suction Cups for Smart Medical Skin. *Adv. Healthc. Mater.* **2016**, *5* (1), 80−87.
(26) Wang, Y.; Kang, V.; Federle, W.; Arzt, E.; Hensel, R. Switchable Underwater Adhesion by Deformable Cupped Microstructures. *Adv. Mater. Interfaces* **2020**, *7* (23), No. 2001269.
(27) Swift, M. D.; Haverkamp, C. B.; Stabile, C. J.; Hwang, D.; Plaut, R. H.; Turner, K. T.; Dillard, D. A.; Bartlett, M. D. Active Membranes on Rigidity Tunable Foundations for Programmable, Rapidly Switchable Adhesion. *Adv. Mater. Technol.* **2020**, *5* (11), No. 2000676.
(28) Wang, T. Y.; Liao, T. Y.; Tzeng, C. S. Phylogeography of The Taiwanese Endemic Hillstream Loaches, Hemimyzon Formosanus and H. Taitungensis (Cypriniformes: Balitoridae). *Zool. Stud.* **2007**, *46* (5), 547−560.
(29) Shih, S. S.; Lee, H. Y.; Chen, C. C. Model-Based Evaluations of Spur Dikes for Fish Habitat Improvement: A Case Study of Endemic Species Varicorhinus Barbatulus (Cyprinidae) and Hemimyzon Formosanum (Homalopteridae) in Lanyang River. *Taiwan. Ecol. Eng.* **2008**, *34* (2), 127−136.
(30) Hiew, S. H.; Mohanram, H.; Ning, L. L.; Guo, J. J.; Sanchez-Ferrer, A.; Shi, X. Y.; Pervushin, K.; Mu, Y. G.; Mezzenga, R.; Miserez, A. A Short Peptide Hydrogel with High Stiffness Induced by 3(10)-Helices to beta-Sheet Transition in Water. *Adv. Sci.* **2019**, *6* (21), No. 1901173.
(31) Guan, Q.; Fang, Y. L.; Wu, X.; Ou, R. W.; Zhang, X. Y.; Xie, H.; Tang, M. Y.; Zeng, G. S. Stimuli Responsive Metal Organic Framework Materials Towards Advanced Smart Application. *Mater. Today* **2023**, *64*, 138−164.
(32) Baniasadi, M.; Yarali, E.; Bodaghi, M.; Zolfagharian, A.; Baghani, M. Constitutive Modeling of Multi-Stimuli-Responsive Shape Memory Polymers with Multi-Functional Capabilities. *Int. J. Mech. Sci.* **2021**, *192*, No. 106082.
(33) Peng, K. Y.; Zhao, Y.; Shahab, S.; Mirzaeifar, R. Ductile Shape-Memory Polymer Composite with Enhanced Shape Recovery Ability. *ACS Appl. Mater. Interfaces* **2020**, *12* (52), 58295−58300.
(34) Son, C.; Kim, S. Dual Adaptation of a Flexible Shape Memory Polymer Adhesive. *ACS Appl. Mater. Interfaces* **2021**, *13* (23), 27656−27662.

https://doi.org/10.1021/acsami.3c15577
ACS Appl. Mater. Interfaces 2023, 15, 56203−56212

(35) Xia, Y. L.; He, Y.; Zhang, F. H.; Liu, Y. J.; Leng, J. S. A Review of Shape Memory Polymers and Composites: Mechanisms, Materials, and Applications. *Adv. Mater.* **2021**, *33* (6), No. 2000713.
(36) Hornat, C. C.; Urban, M. W. Shape Memory Effects in Self-Healing Polymers. *Prog. Polym. Sci.* **2020**, *102*, No. 101208.
(37) Lorwanishpaisarn, N.; Kasemsiri, P.; Jetsrisuparb, K.; Knijnenburg, J. T. N.; Hiziroglu, S.; Pongsa, U.; Chindaprasirt, P.; Uyama, H. Dual-Responsive Shape Memory and Self-Healing Ability of A Novel Copolymer from Epoxy/Cashew Nut Shell Liquid and Polycaprolactone. *Polym. Test* **2020**, *81*, No. 106159.
(38) Leverant, C. J.; Leo, S. Y.; Cordoba, M. A.; Zhang, Y. F.; Charpota, N.; Taylor, C.; Jiang, P. Reconfigurable Anticounterfeiting Coatings Enabled by Macroporous Shape Memory Polymers. *ACS Appl. Polym. Mater.* **2019**, *1* (1), 36−46.
(39) Fang, Y.; Leo, S. Y.; Ni, Y. L.; Wang, J. Y.; Wang, B. C.; Yu, L.; Dong, Z.; Dai, Y. Q.; Basile, V.; Taylor, C.; et al. Reconfigurable Photonic Crystals Enabled by Multistimuli-Responsive Shape Memory Polymers Possessing Room Temperature Shape Processability. *ACS Appl. Mater. Interfaces* **2017**, *9* (6), 5457−5467.
(40) Sekiguchi, K.; Katsumata, K.-i.; Segawa, H.; Nakanishi, T.; Yasumori, A. Effects of Particle Size, Concentration and Pore Size on The Loading Density of Silica Nanoparticle Monolayer Arrays on Anodic Aluminum Oxide Substrates Prepared by The Spin-Coating Method. *Mater. Chem. Phys.* **2022**, *277*, No. 125465.
(41) Xie, T. T.; Wang, H.; Chen, K.; Li, F. Y.; Zhao, S. C.; Sun, H. X.; Yang, X. J.; Hou, Y. F.; Li, P.; Niu, J. S.; et al. High-Performance Polyethyleneimine Based Reverse Osmosis Membrane Fabricated via Spin-Coating Technology. *J. Membr. Sci.* **2023**, *668*, No. 121248.
(42) Fernandes, R. S.; Raimundo, I. M.; Pimentel, M. F. Revising The Synthesis of Stober Silica Nanoparticles: A Multivariate Assessment Study on The Effects of Reaction Parameters on The Particle Size. *Colloid Surf. A-Physicochem. Eng. Asp.* **2019**, *577*, 1−7.
(43) Chen, Y.-C.; Yang, H. Octopus-Inspired Assembly of Nanosucker Arrays for Dry/Wet Adhesion. *ACS Nano* **2017**, *11* (6), 5332−5338.
(44) Jiang, P.; Prasad, T.; McFarland, M. J.; Colvin, V. L. Two-Dimensional Nonclose-Packed Colloidal Crystals Formed by Spin-Coating. *Appl. Phys. Lett.* **2006**, *89* (1), No. 011908.
(45) Jiang, P.; McFarland, M. J. Large-Scale Fabrication of Wafer-Size Colloidal Crystals, Macroporous Polymers and Nanocomposites by Spin-Coating. *J. Am. Chem. Soc.* **2004**, *126* (42), 13778−13786.
(46) Tseng, H.-Y.; Chen, Y.-H.; Chen, R.-U.; Yang, H. Reversibly Erasable Broadband Omnidirectional Antireflection Coatings Inspired by Inclined Conical Structures on Blue-Tailed Forest Hawk Dragonfly Wings. *ACS Appl. Mater. Interfaces* **2020**, *12* (9), 10883−10892.
(47) Chen, Y.-C.; Huang, Z.-H.; Yang, H. Cicada-Wing-Inspired Self-Cleaning Antireflection Coatings on Polymer Substrates. *ACS Appl. Mater. Interfaces* **2015**, *7* (45), 25495−25505.
(48) Kothary, P.; Dou, X.; Fang, Y.; Gu, Z.; Leo, S.-Y.; Jiang, P. Superhydrophobic Hierarchical Arrays Fabricated by A Scalable Colloidal Lithography Approach. *J. Colloid Interface Sci.* **2017**, *487*, 484−492.
(49) Min, W.-L.; Jiang, P.; Jiang, B. Large-Scale Assembly of Colloidal Nanoparticles and Fabrication of Periodic Subwavelength Structures. *Nanotechnology.* **2008**, *19*, No. 475604.
(50) Leverant, C. J.; Leo, S.-Y.; Cordoba, M. A.; Zhang, Y.; Charpota, N.; Taylor, C.; Jiang, P. Reconfigurable Anticounterfeiting Coatings Enabled by Macroporous Shape Memory Polymers. *ACS Appl. Polym. Mater.* **2019**, *1* (1), 36−46.
(51) Fang, Y.; Leo, S.-Y.; Ni, Y.; Wang, J.; Wang, B.; Yu, L.; Dong, Z.; Dai, Y.; Basile, V.; Taylor, C.; Jiang, P. Reconfigurable Photonic Crystals Enabled by Multistimuli-Responsive Shape Memory Polymers Possessing Room Temperature Shape Processability. *ACS Appl. Mater. Interfaces* **2017**, *9* (6), 5457−5467.
(52) Zhang, Y.; Lyu, X.; Ni, Y.; Li, D.; Leo, S.-Y.; Chen, Y.; Jiang, P.; Taylor, C. R. Switchable friction coefficient on shape memory photonic crystals. *MRS Adv.* **2020**, *5* (14−15), 757−763.
(53) Wang, G. F.; Liu, Y.; Zu, B. Y.; Lei, D.; Guo, Y. A.; Wang, M. M.; Dou, X. C. Reversible Adhesive Hydrogel with Enhanced Sampling Efficiency Boosted by Hydrogen Bond and Van Der Waals Force for Visualized Detection. *Chem. Eng. J.* **2023**, *455*, No. 140493.
(54) Fang, Y.; Ni, Y.; Leo, S.-Y.; Taylor, C.; Basile, V.; Jiang, P. Reconfigurable Photonic Crystals Enabled by Pressure-Responsive Shape-Memory Polymers. *Nat. Commun.* **2015**, *6* (1), 7416.
(55) Fang, Y.; Ni, Y.; Leo, S.-Y.; Wang, B.; Basile, V.; Taylor, C.; Jiang, P. Direct Writing of Three-Dimensional Macroporous Photonic Crystals on Pressure-Responsive Shape Memory Polymers. *ACS Appl. Mater. Interfaces* **2015**, *7* (42), 23650−23659.
(56) Lendlein, A.; Kelch, S. Shape-Memory Polymers. *Angew. Chem., Int. Ed.* **2004**, *41*, 2034−2057.
(57) Espinha, A.; Concepcion Serrano, M.; Blanco, A.; Lopez, C. Thermoresponsive Shape-Memory Photonic Nanostructures. *Adv. Opt. Mater.* **2014**, *2*, 516−521.
(58) Xu, H.; Yu, C.; Wang, S.; Malyarchuk, V.; Xie, T.; Rogers, J. A. Deformable, Programmable, and Shape-Memorizing Micro-Optics. *Adv. Funct. Mater.* **2013**, *23*, 3299−3306.

https://doi.org/10.1021/acsami.3c15577
ACS Appl. Mater. Interfaces 2023, 15, 56203−56212